Rotationally resolved photoelectron spectra in resonance enhanced multiphoton ionization of Rydberg states of NH

Kwanghsi Wang, J. A. Stephens, V. McKoy, E. de Beer, C. A. de Lange, and N. P. C. Westwood

Citation: The Journal of Chemical Physics **97**, 211 (1992); doi: 10.1063/1.463619
View online: http://dx.doi.org/10.1063/1.463619
View Table of Contents: http://scitation.aip.org/content/aip/journal/jcp/97/1?ver=pdfcov
Published by the AIP Publishing

Rotationally resolved photoelectron spectra in resonance enhanced multiphoton ionization of Rydberg states of NH

Kwanghsi Wang, J. A. Stephens, and V. McKoy
Arthur Amos Noyes Laboratory of Chemical Physics,[a] *California Institute of Technology, Pasadena, California 91125*

E. de Beer, C. A. de Lange, and N. P. C. Westwood[b]
Laboratory for Physical Chemistry, University of Amsterdam, Nieuwe Achtergracht 127, 1018 WS Amsterdam, The Netherlands

(Received 20 February 1992; accepted 17 March 1992)

Results of combined theoretical and experimental studies of photoelectron spectra resulting from (2 + 1) resonance enhanced multiphoton ionization (REMPI) via the $f\,^1\Pi(3p\sigma)$, $g\,^1\Delta(3p\pi)$, and $h\,^1\Sigma^+(3p\pi)$ Rydberg states of NH are reported. The overall agreement between these calculated and measured spectra is encouraging. Strong $\Delta N = N^+ - N' =$ even peaks, particularly for $\Delta N = 0$, are observed in these spectra. Low-energy Cooper minima are predicted to occur in the $\ell = 2$ wave of the $k\pi(^1\Sigma^+)$, $k\pi(^1\Sigma^-)$, and $k\pi(^1\Delta)$ photoelectron channels for the f state, the $k\pi(^1\Delta)$, $k\delta(^1\Pi)$, and $k\delta(^1\Phi)$ channels for the g state, and the $k\pi(^1\Sigma^+)$ and $k\delta(^1\Pi)$ channels for the h state of NH. Depletion of the d wave ($\ell = 2$) contributions to the photoelectron matrix element in the vicinity of these Cooper minima subsequently enhances the relative importance of the odd ℓ waves. The observed ΔN transitions are also affected by strong ℓ mixing in the electronic continuum induced by the nonspherical molecular potential. Interference of continuum waves between degenerate ionization channels also determines the spectral pattern observed for photoionization of the $f\,^1\Pi$ state of NH. Photoelectron angular distributions and the angular momentum compositions of photoelectron matrix elements provide further insight into the origin of these Cooper minima.

I. INTRODUCTION

Effects of Cooper minima[1,2] on rotationally resolved photoelectron spectra have recently been observed for (2 + 1) resonance enhanced multiphoton ionization (REMPI) via the $D\,^2\Sigma^-(3p\sigma)$ state of OH (Ref. 3), and the $D\,^2\Sigma^+(3p\sigma)$ Rydberg state of NO (Refs. 4 and 5). These photoelectron spectra reveal strong $\Delta N = N^+ - N' =$ even transitions, particularly for $\Delta N = 0$, in contrast to the expected $\Delta N =$ odd transitions for photoionization of a $3p\sigma$ orbital. Here N^+ and N' are the total angular momentum (excluding spin) of the ionic and intermediate states, respectively. These rotational ion distributions for OH (Ref. 3) and NO (Ref. 5) have been interpreted as arising from Cooper minima in the dipole-allowed ionization channels. Recently, de Beer *et al.* have reported rotationally resolved photoelectron spectra for (2 + 1) REMPI via the $f\,^1\Pi(3p\sigma)$ and $g\,^1\Delta(3p\pi)$ Rydberg states of NH (Ref. 6), which also show unusual $\Delta N =$ even peaks. A systematic theoretical investigation of the underlying photoionization dynamics of these photoelectron spectra is clearly desirable.

The presence of Cooper minima in photoionization of excited states of diatomic molecules was first predicted by Stephens and McKoy[7] for (3 + 1) REMPI via the $D\,^2\Sigma^-$ Rydberg state of OH. Together with orbital evolution of the $3p\sigma$ orbital with internuclear distance, non-Franck–Condon effects in the vibrationally resolved photoelectron spectra were discussed.[7,8] The occurrence of the Cooper minimum was shown to result in the prominent $\Delta N = 0$ peak observed in the rotationally resolved photoelectron spectra.[3,5] Cooper minima have also been predicted for (3 + 1) REMPI via the $3\,^3\Pi(3p\sigma)$ Rydberg state of NH, resulting in non-Franck–Condon vibrational distributions[9] and unusual rotational branching ratios[10] for various vibrational transitions. Recently, Wang *et al.*[5] have identified and systematically investigated the role of Cooper minima on photoelectron spectra for (2 + 1′) REMPI via the $D\,^2\Sigma^+(3p\sigma)$ and $C\,^2\Pi(3p\pi)$ Rydberg states of NO. These minima lead to strong kinetic energy dependence of the rotational ion distributions and photoelectron angular distributions. Cooper minima in (2 + 1′) REMPI spectra via the $H\,^2\Sigma^+(3d,4s)$ Rydberg state of NO were also first predicted to have marked effects on the rotational branching ratios, and, in fact, to allow production of molecular ions in specific rotational levels.[11] The generality and implications of Cooper minima in REMPI processes are just emerging.

With the REMPI technique, a single rotational level of the resonant intermediate state is selected so that only a few rotational levels of the ion are accessed, resulting in substantial simplification in the photoelectron spectra. Thus, parity selection rules,[10,12–14] which govern the changes of rota-

[a] Contribution No. 8577.
[b] On leave from the Guelph-Waterloo Center for Graduate Work in Chemistry, University of Guelph, Guelph, Ontario, N1G 2W1, Canada.

tional angular momentum ΔN upon ionization, are important in the interpretation of these spectra and for a qualitative understanding of the photoelectron dynamics. For example, they successfully attributed the unexpected peaks observed in REMPI spectra via the D Rydberg states of OH and NO to odd partial wave contributions to the photoelectron matrix element.[3,5] These odd partial waves are produced via strong ℓ mixing in the electronic continuum and their relative strengths are further enhanced by the formation of Cooper minima.

In this paper we present calculated and measured photoelectron spectra resulting from (2 + 1) REMPI of NH via the $f\,^1\Pi$, $g\,^1\Delta$, and $h\,^1\Sigma^+$ Rydberg states. Cooper minima are predicted to occur in ionization channels for these Rydberg states and are seen to exert a strong influence on the rotationally resolved photoelectron spectra. To provide further insight into these spectra, we also present calculated photoelectron angular distributions.

II. EXPERIMENTAL DETAILS

The experimental arrangement has been described previously.[15] Briefly, the experiments were performed using a frequency-doubled excimer-pumped dye laser (Lumonics Inc.) at a repetition rate of 30 Hz. The dye laser was operated with dyes *C*-500 and *C*-540. The dye laser output was frequency doubled using a β-BaB_2O_4 crystal. The frequency-doubled laser output was focused (f.l. 25 mm) into the ionization region of a "magnetic bottle" spectrometer, where it interrogates an effusive jet of HN_3 vapor. The spectrometer's original design[16] has been modified to allow the study of reactive and transient species. With this spectrometer, electron kinetic energies are measured by means of a time-of-flight technique with 50% collection efficiency and a resolution of 6–8 meV. As the spectrometer has an acceptance angle of 2π steradians, it has a very high sensitivity, but no information on the photoelectron angular distributions can be obtained. The dye laser was calibrated in the visible using optogalvanic lines of Ne, excited in a hollow cathode discharge. REMPI signals of N atoms, produced as a by-product in the photodissociation process, provided an internal calibration. The energy scale of the photoelectron spectra was calibrated using (2 + 1) REMPI of Xe at 249.6 nm.

NH radicals were produced by photodissociation of HN_3 in the wavelength region 255–285 nm. HN_3 was generated by warming an intimate 5:1 solid mixture of stearic acid and NaN_3 contained in a Pyrex section of the evacuable supply line leading to the effusive beam source. The experiments were carried out with one laser only, and photodissociation and subsequent REMPI of the radicals generated took place within one laser pulse. The photofragmentation dynamics of HN_3 has been studied in detail previously[17,18] at various photolysis wavelengths (248, 266, 283, and 308 nm) relevant for the present work.

The excess energy of this one-photon process is distributed over all degrees of freedom of the fragments formed. Since N_2 is formed in its electronic and vibrational ground state $X\,^1\Sigma_g^+$, the NH fragments must be formed in a spin-singlet state. In practice, NH is formed exclusively in the spin-allowed $a\,^1\Delta$ state, 12 589 cm^{-1} above its $X\,^3\Sigma^-$ ground state, with a statistical population in the Λ-doublet components. In the present experiments, the laser bandwidth of $\sim$0.5 cm^{-1} is insufficient to resolve the Λ doublet in the initial $a\,^1\Delta$ and intermediate $f\,^1\Pi$ and $g\,^1\Delta$ states. In the $X\,^2\Pi$ ionic state the photoelectron kinetic energy resolution is insufficient to resolve the Λ doublets. The population of the vibrational levels in the $a\,^1\Delta$ state has been studied at 266 nm and $v = 0$–3 are found to be populated.[18] Surprisingly, the translational ($\sim$5800 cm^{-1}) and rotational ($\sim$700 cm^{-1}) energies of the NH fragments show little variation with the photolysis wavelength. The rotational alignment was found to be small at all photolysis wavelengths studied. In the present photoelectron experiments the translational energy of the NH fragments leads to a Doppler broadening of $\sim$30 meV. Despite this broadening, the excitation to higher rotational states is such that rotationally resolved photoelectron spectra can be recorded.

III. THEORY AND NUMERICAL DETAILS

A. Cross sections for (2+1) REMPI

The (2 + 1) REMPI processes via the $f\,^1\Pi(3p\sigma)$, $g\,^1\Delta(3p\pi)$, and $h\,^1\Sigma^+(3p\pi)$ intermediate states of NH are summarized as follows:

$$\mathrm{NH}[a\,^1\Delta(v_0=0,J_0)] \xrightarrow{2\omega} \mathrm{NH}^*[f\,^1\Pi(v=0,J=N)] \xrightarrow{\omega} \mathrm{NH}^+[X\,^2\Pi(v^+,J^+,N^+)] + e^-(\mathbf{k}), \quad (1a)$$

$$\mathrm{NH}[a\,^1\Delta(v_0=0,J_0)] \xrightarrow{2\omega} \mathrm{NH}^*[g\,^1\Delta(v=0,1,J=N)] \xrightarrow{\omega} \mathrm{NH}^+[X\,^2\Pi(v^+,J^+,N^+)] + e^-(\mathbf{k}), \quad (1b)$$

and

$$\mathrm{NH}[a\,^1\Delta(v_0=0,J_0)] \xrightarrow{2\omega} \mathrm{NH}^*[h\,^1\Sigma^+(v=0,J=N)] \xrightarrow{\omega} \mathrm{NH}^+[X\,^2\Pi(v^+,J^+,N^+)] + e^-(\mathbf{k}). \quad (1c)$$

For linearly polarized light, ionization originating from each of the $(2J_0 + 1)$ magnetic sublevels of the initial state forms an independent channel under collision-free conditions. Therefore, the rotationally resolved differential cross section for photoionization of a rotational level of the intermediate state can be expressed as

$$\frac{d\sigma}{d\Omega} \propto \sum_{M_J M_{J^+}} \rho_{M_J M_J} |\Gamma_{M_J M_{J^+}}|^2 = \frac{\sigma}{4\pi}\left[1 + \sum_L \beta_{2L} P_{2L}(\cos\theta)\right], \quad (2)$$

where σ is the total cross section, β_{2L} the asymmetry parameters, θ the angle between the photoelectron and the polar-

ization vector of the laser, and $P_{2L}(\cos\theta)$ the Legendre polynomials.

In Eq. (2), $\rho_{M_J M_J}$ is the population of a specific M_J level of the intermediate state created by two-photon excitation. For rotational branches other than Q branches, $\rho_{M_J M_J}$ is a product of a 3-j symbol and a rotational line strength B,[19]

$$\rho_{M_J M_J} = \mathcal{N}\begin{pmatrix} J & 2 & J_0 \\ -M_J & 0 & M_J \end{pmatrix}^2 B, \tag{3}$$

where $\mathcal{N}$ is a normalization constant. The rotational line strength B for two- and three-photon excitation of diatomic molecules has been tabulated by Halpern *et al.*[19] However, in the case of Q branches, $\rho_{M_J M_J}$ becomes[20]

$$\rho_{M_J M_J} = \mathcal{N}\left|\begin{pmatrix} J & 2 & J_0 \\ -M_J & 0 & M_J \end{pmatrix} B_2 + B_0\right|^2. \tag{4}$$

Note that B_0 contains no polarization information, but is crucial in determining the population $\rho_{M_J M_J}$ of the intermediate state for (2 + 1) REMPI via Q rotational branches. The evaluation of the B_2 and B_0 factors requires a summation over all possible paths and dipole-allowed virtual states in the two-photon excitation step. $|\Gamma_{M_J M_{J^+}}|^2$ of Eq. (2) is the probability for photoionization of the M_J level of the intermediate state leading to the M_{J^+} level of the ion. An expression for $\Gamma_{M_J M_{J^+}}$ has been derived by Wang and McKoy[10] by explicitly considering the spin coupling associated with multiplet-specific final-state wave functions and intermediate coupling schemes between Hund's cases (a) and (b) for describing the resonant and ionic states.

Parity selection rules,[10,12-14] governing changes of rotational angular momentum upon photoionization, have been derived previously and are of the form

$$\Delta J + \Delta S + \Delta p + \Delta q + \ell = \text{even}, \tag{5}$$

for Hund's case (a) coupling scheme, where $\Delta J = J^+ - J$, $\Delta S = S^+ - S$, $\Delta p = p^+ - p$, and $\Delta q = q^+ - q$. In Eq. (5), J denotes the total angular momentum, S the total spin, ℓ a partial-wave component of the photoelectron, p the parity index of e/f levels,[10,21] and q the index for Σ^- symmetry.[10,12] In the Hund's case (b) limit, Eq. (5) reduces to[10,12-14]

$$\Delta N + \Delta p + \Delta q + \ell = \text{odd}. \tag{6}$$

B. Multiplet-specific wave functions and potentials

There are four dipole-allowed channels for photoionization of the $5\sigma(3p\sigma)$ orbital of the $f\,^1\Pi$ state and the $2\pi(3p\pi)$ orbital of the $g\,^1\Delta$ state of NH, respectively. The corresponding multiplet-specific final-state wave functions for the $f\,^1\Pi$ state are given by

$$\Psi(^1\Pi) = \frac{1}{\sqrt{2}}\left[|(\text{core})1\pi_+\ \overline{k\sigma}| - |(\text{core})\ \overline{1\pi}_+ k\sigma|\right], \tag{7a}$$

$$\Psi(^1\Sigma^+) = \frac{1}{2}\left[|(\text{core})1\pi_+\ \overline{k\pi}_-| - |(\text{core})\ \overline{1\pi}_+ k\pi_-| + |(\text{core})1\pi_-\ \overline{k\pi}_+| - |(\text{core})\ \overline{1\pi}_- k\pi_+|\right], \tag{7b}$$

$$\Psi(^1\Sigma^-) = \frac{1}{2}\left[|(\text{core})1\pi_+\ \overline{k\pi}_-| - |(\text{core})\ \overline{1\pi}_+ k\pi_-| - |(\text{core})1\pi_-\ \overline{k\pi}_+| + |(\text{core})\ \overline{1\pi}_- k\pi_+|\right], \tag{7c}$$

and

$$\Psi(^1\Delta) = \frac{1}{\sqrt{2}}\left[|(\text{core})1\pi_+\ \overline{k\pi}_+| - |(\text{core})\ \overline{1\pi}_+ k\pi_+|\right], \tag{7d}$$

where (core) = $1\sigma^2 2\sigma^2 3\sigma^2$. The corresponding multiplet-specific final-state wave functions for the $g\,^1\Delta$ state are

$$\Psi(^1\Pi) = \frac{1}{\sqrt{2}}\left[|(\text{core})1\pi_+\ \overline{k\sigma}| - |(\text{core})\ \overline{1\pi}_+ k\sigma|\right], \tag{8a}$$

$$\Psi(^1\Delta) = \frac{1}{\sqrt{2}}\left[|(\text{core})1\pi_+\ \overline{k\pi}_+| - |(\text{core})\ \overline{1\pi}_+ k\pi_+|\right], \tag{8b}$$

$$\Psi(^1\Pi) = \frac{1}{\sqrt{2}}\left[|(\text{core})1\pi_-\ \overline{k\delta}_+| - |(\text{core})\ \overline{1\pi}_- k\delta_+|\right], \tag{8c}$$

and

$$\Psi(^1\Phi) = \frac{1}{\sqrt{2}}\left[|(\text{core})1\pi_+\ \overline{k\delta}_+| - |(\text{core})\ \overline{1\pi}_+ k\delta_+|\right]. \tag{8d}$$

There are three dipole-allowed channels for photoionization of the $2\pi(3p\pi)$ orbital of the $h\,^1\Sigma^+$ Rydberg state of NH. The corresponding multiplet-specific final-state wave functions are

$$\Psi(^1\Sigma^+) = \frac{1}{2}\left[|(\text{core})1\pi_-\ \overline{k\pi}_+| - |(\text{core})\ \overline{1\pi}_- k\pi_+| + |(\text{core})1\pi_+\ \overline{k\pi}_-| - |(\text{core})\ \overline{1\pi}_+ k\pi_-|\right], \tag{9a}$$

$$\Psi(^1\Pi) = \frac{1}{\sqrt{2}}\left[|(\text{core})1\pi_+\ \overline{k\sigma}| - |(\text{core})\ \overline{1\pi}_+ k\sigma|\right], \tag{9b}$$

and

$$\Psi(^1\Pi) = \frac{1}{\sqrt{2}}\left[|(\text{core})1\pi_-\ \overline{k\delta}_+| - |(\text{core})\ \overline{1\pi}_- k\delta_+|\right]. \tag{9c}$$

Within the frozen-core Hartree–Fock approximation,

the one-particle Schrödinger equation for the photoelectron orbital ϕ_k can be shown to have the form[22,23]

$$P\Big[f+\sum_{i=\text{core}}(2J_i-K_i)+a_nJ_n+b_nK_n+\alpha S''_{1\pi}+\beta S'_{1\pi}-\epsilon\Big]P|\phi_k\rangle=0, \tag{10}$$

where J_i and K_i are the Coulomb and exchange operators, respectively, and P is a projection operator which enforces orthogonality of the continuum orbital to the occupied orbitals.[22,23] The photoelectron kinetic energy is given by $\epsilon=(1/2)k^2$. The operators S'' and S' are defined as

$$S''_\pi\phi_+(\mathbf{r}_1)=\phi_-(\mathbf{r}_1)\int d^3\mathbf{r}_2\,[\pi_-(\mathbf{r}_2)^*]\,\frac{1}{r_{12}}\,\pi_+(\mathbf{r}_2), \tag{11}$$

and

$$S'_\pi\phi_+(\mathbf{r}_1)=\pi_+(\mathbf{r}_1)\int d^3\mathbf{r}_2\,[\pi_-(\mathbf{r}_2)^*]\,\frac{1}{r_{12}}\,\phi_-(\mathbf{r}_2). \tag{12}$$

The one-electron operator f in Eq. (10) is

$$f=-\frac{1}{2}\nabla_i^2-\sum_\alpha\frac{Z_\alpha}{r_{i\alpha}}, \tag{13}$$

where Z_α is a nuclear charge. The coefficients α, β, a_n, and b_n for the static-exchange potential of Eq. (10) associated with the $1\pi_+$ and $1\pi_-$ orbitals of the f, g, and h states of NH are listed in Table I.

C. Numerical details

We use the improved virtual orbital (IVO) method[24] to obtain the wave functions of the $f\,^1\Pi(3p\sigma)$, $g\,^1\Delta(3p\pi)$, and $h\,^1\Sigma^+(3p\pi)$ Rydberg states of NH. The core orbitals are taken to be those of the fully relaxed core of the ion. The orbital basis used in these calculations consists of a $[4s3p]$ contraction of the $(9s5p)$ primitive Cartesian Gaussian basis of Dunning[25] augmented with one s ($\alpha=0.1$), one p ($\alpha=0.085$), and two d ($\alpha=1.4836$ and 0.4691) functions on the nitrogen atom. On the hydrogen we used the $[3s1p]$ contraction of the $(4s2p)$ primitive Cartesian Gaussian basis of Dunning[25] augmented with one s ($\alpha=0.1$) and three p ($\alpha=0.95$, 0.25, and 0.1) functions. This basis is further augmented with five s ($\alpha=0.055$, 0.028, 0.012, 0.0066, and 0.002), five p ($\alpha=0.048$, 0.025, 0.012, 0.0051, and 0.002), and three d ($\alpha=0.08$, 0.015, and 0.0032) functions on the center of mass (CM). At its equilibrium internuclear distance of $R_e=2.06\,a_0$,[6] the self-consistent-field (SCF) energy of the $f\,^1\Pi$ state of NH in this basis is $-54.595\,048$ a.u. The total energy is $-54.591\,828$ a.u. for the $g\,^1\Delta$ state at $R_e=2.02\,a_0$,[6] and $-54.588\,348$ a.u. for the $h\,^1\Sigma^+$ state at $R_e=2.04\,a_0$.[26] The $3p\sigma(5\sigma)$ orbital of the $f\,^1\Pi$ state has a rapid orbital evolution with internuclear distance from predominant $3p$ character at smaller internuclear distance to $3s$ character at larger R.[27,28] For example, the single-center expansion of the 5σ orbital around the center of mass has the following partial wave compositions: 14.7% s, 82.8% p, and 2.5% d at $R=1.25\,a_0$, 24.4% s, 67.4% p, 8.1% d, and 0.1% f at $R=2.05\,a_0$, and 83.0% s, 4.3% p, 10.9% d, 1.1% f, and 0.4% $g(\ell=4)$ at $R=3.0\,a_0$. These are similar to those of the $3p\sigma$ orbital of the $3\,^3\Pi$ state.[9] However, the composition of the $3p\pi$ orbital of the $g\,^1\Delta$ and $h\,^1\Sigma^+$ states varies only slightly with internuclear distance. The $3p\pi$ orbital of the g state has 96.5% p and 3.5% d character at $2.02\,a_0$. The vibrational wave functions for the f, g, and h states of NH were obtained by numerical integration over a range of $1.25\leqslant R\leqslant 3.5\,a_0$. Eleven internuclear distances were explicitly included in the calculations. We use the potential curves obtained from our SCF calculations on NH^+ and the IVO calculations for NH Rydberg states, with the calculated R_e values slightly shifted to the experimental values quoted above.

To obtain the photoelectron orbitals we have used an iterative procedure, based on the Schwinger variational principle,[22,23] to solve the Lippmann–Schwinger equation associated with Eq. (10). In this procedure, the static-exchange potential is approximated by

$$U(\mathbf{r},\mathbf{r}')=\sum_{ij}\langle\mathbf{r}|U|\alpha_i\rangle(U^{-1})_{ij}\langle\alpha_j|U|\mathbf{r}'\rangle, \tag{14}$$

where the matrix U^{-1} is the inverse of the matrix with elements $U_{ij}=\langle\alpha_i|U|\alpha_j\rangle$ and the α's are discrete basis functions such as Cartesian or spherical Gaussian functions. The basis sets used in the separable expansion of Eq. (14) can be found in Ref. 9. U is twice the static-exchange potential in Eq. (10) with the long-range Coulomb potential removed. The Lippmann–Schwinger equation with this separable potential $U(\mathbf{r},\mathbf{r}')$ can be readily solved yielding approximate photoelectron orbitals $\phi_k^{(0)}$. These solutions can be iteratively improved to yield converged photoelectron orbitals ϕ_k to the Lippmann–Schwinger equation containing the full static-exchange potential. In this study, two iterations provided converged solutions of Eq. (10). Other details of the calculation can be obtained from Ref. 9.

TABLE I. Coefficients of the static-exchange potential in Eq. (10).

Resonant state	Channel[a,b]	a_n/b_n		α/β
		$1\pi_+$	$1\pi_-$	
$f\,^1\Pi$	$k\sigma(^1\Pi)$	1/1	0/0	0/0
	$k\pi(^1\Sigma^+)$	0/0	1/1	1/1
	$k\pi(^1\Sigma^-)$	0/0	1/1	−1/−1
	$k\pi(^1\Delta)$	1/1	0/0	0/0
$g\,^1\Delta$	$k\sigma(^1\Pi)$	1/1	0/0	0/0
	$k\pi(^1\Delta)$	1/1	0/0	0/0
	$k\delta(^1\Pi)$	0/0	1/1	0/0
	$k\delta(^1\Phi)$	1/1	0/0	0/0
$h\,^1\Sigma^+$	$k\sigma(^1\Pi)$	1/1	0/0	0/0
	$k\pi(^1\Sigma^+)$	0/0	1/1	1/1
	$k\delta(^1\Pi)$	0/0	1/1	0/0

[a] Channel designates symmetry of the ion plus photoelectron system.
[b] See Eqs. (7)–(9).

IV. RESULTS AND DISCUSSION

A. (2+1) REMPI via the $f\,^1\Pi$ Rydberg state of NH

To understand the underlying dynamics of these rotationally resolved photoelectron spectra, it is useful to exam-

ine the angular momentum composition of the photoionization matrix elements. Figure 1 shows the magnitude of the (incoming-wave normalized) partial wave dipole amplitude $|D_\ell^{(-)}|$ as a function of photoelectron kinetic energy for the photoionization channels $3p\sigma \rightarrow k\sigma(^1\Pi)$ [Fig. 1(a)], $3p\sigma \rightarrow k\pi(^1\Sigma^+)$ [Fig. 1(b)], $3p\sigma \rightarrow k\pi(^1\Sigma^-)$ [Fig. 1(c)], and $3p\sigma \rightarrow k\pi(^1\Delta)$ [Fig. 1(d)] via the $f\,^1\Pi(3p\sigma)$ Rydberg state of NH. Three Cooper minima, which are due to sign changes in the $\ell = 2$ (d wave) components around the minimum in $|D_\ell^{(-)}|$, are clearly seen at kinetic energy around 0.5 eV for the $k\pi(^1\Sigma^-)$ channel and around 1.8 eV for the $k\pi(^1\Sigma^+)$ and $k\pi(^1\Delta)$ channels. The actual sign changes in the dipole matrix elements are seen in the principal-value (standing-wave normalized) dipole amplitude D_ℓ^P (Refs. 8, 22, and 23), as shown in the insets of Figs. 1(b)–(d) for the $\ell = 2$ wave. The energy positions of these minima in $|D_\ell^{(-)}|$ may differ somewhat from those of Cooper zeros in D_ℓ^P. This is apparent in the $k\pi(^1\Sigma^+)$ and $k\pi(^1\Delta)$ channels. These shifts are due to strong ℓ mixing in the electronic continuum via the renormalization of D_ℓ^P to $D_\ell^{(-)}$. A less pronounced minimum is also seen in the $\ell = 2$ wave around 0.5 eV for the $k\sigma(^1\Pi)$ channel. However, the corresponding D_ℓ^P does not show a distinct sign change within the energy range studied (not shown). Figure 1 also shows that the multiplet-specific potentials play a role in determining the detailed position of the minimum in $|D_\ell^{(-)}|$ [cf. Figs. 1(b) and 1(d)], as well as in rescattering in the continuum state [Figs. 1(b)–(d)]. Note that the scale for each ionization channel is different. The odd partial waves, particularly p and f waves, are dominant in the vicinities of minima in $|D_\ell^{(-)}|$.

In Fig. 2 we show the measured[6] [Fig. 2(a)] and calculated [Fig. 2(b)] photoelectron spectra along with calculated photoelectron angular distributions [Fig. 2(c)] for (2 + 1) REMPI via the $R(12)$ rotational branch of the $f\,^1\Pi(3p\sigma)$ Rydberg state of NH for the 0–0 and 0–1 vibrational bands. The Λ doublets of the initial, intermediate, and ionic states are not resolved in these spectra. The calculated rotational ion distributions are convoluted with a Gaussian detection function having a full width at half-maximum (FWHM) of 30 meV. The agreement between the calculated and measured spectra is encouraging. When NH radicals are formed by UV photolysis of HN_3, it is known[17] that the e and f components of the $a\,^1\Delta$ state are equally populated and that the alignment is small. Hence, in our calculations we assumed equal population of all M_{J_0} levels. The relative population of M_J levels (alignment) of the e and f components of the $f\,^1\Pi$ state is determined from Eq. (3).

In Fig. 2, a predominant $\Delta N = 0$ ($N^+ = 13$) transition

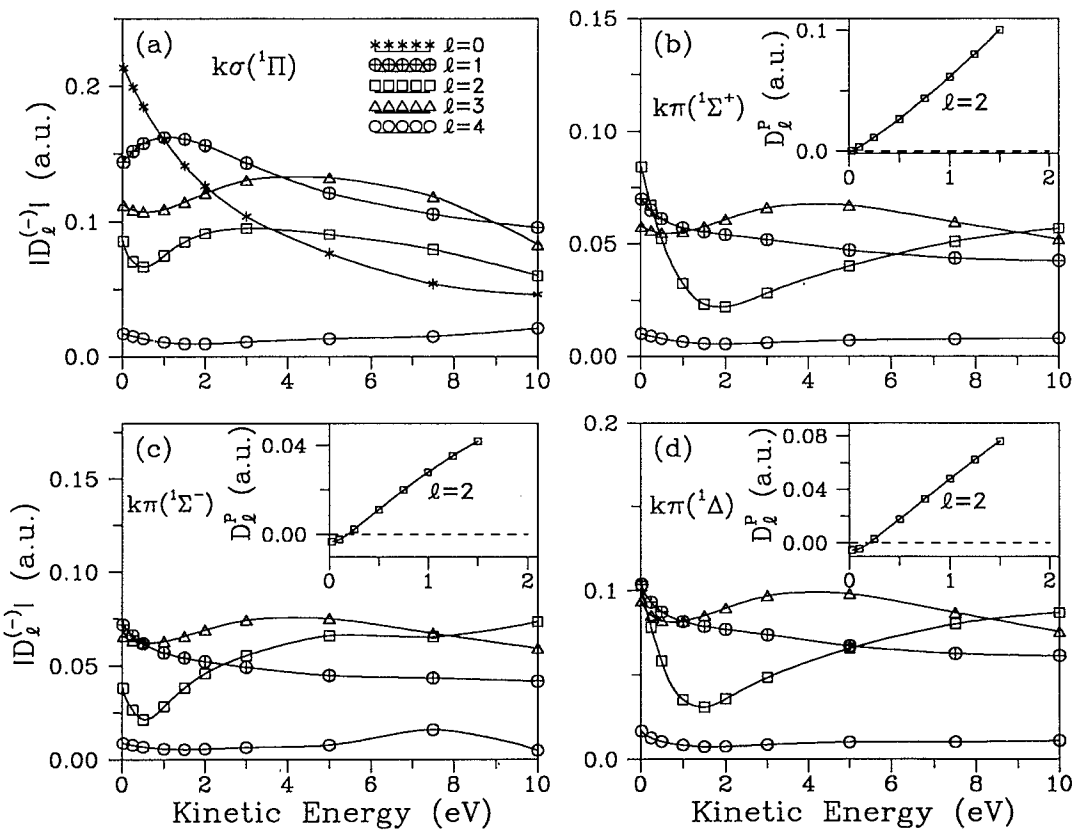

FIG. 1. Magnitude $|D_\ell^{(-)}|$ of the partial wave components of the photoelectron matrix element for photoionization of the $f\,^1\Pi(3p\sigma)$ Rydberg state of NH for the (a) $3p\sigma \rightarrow k\sigma(^1\Pi)$, (b) $3p\sigma \rightarrow k\pi(^1\Sigma^+)$, (c) $3p\sigma \rightarrow k\pi(^1\Sigma^-)$, and (d) $3p\sigma \rightarrow k\pi(^1\Delta)$ ionization channels. The inset shows the principal-value dipole amplitude D_ℓ^P for the $\ell = 2$ component.

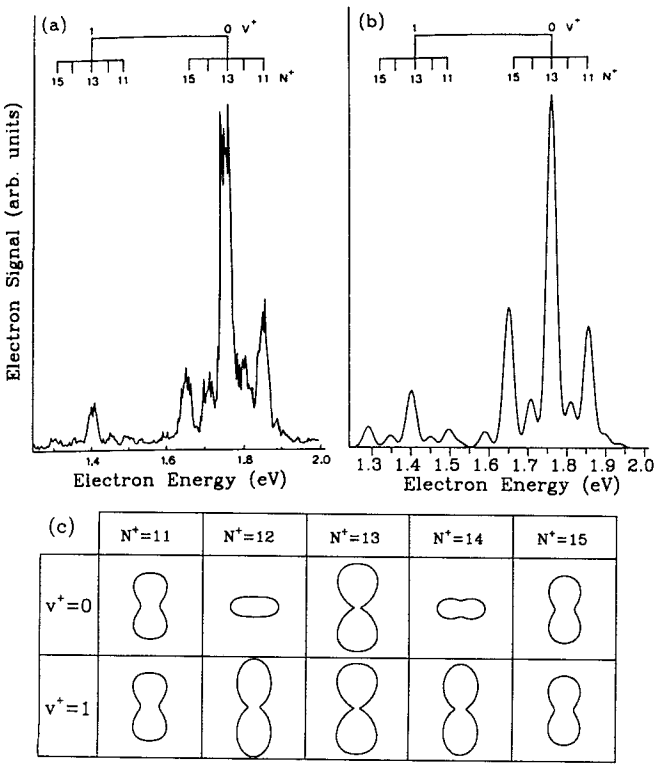

FIG. 2. The (a) measured and (b) calculated photoelectron spectra along with the (c) calculated photoelectron angular distributions resulting from (2 + 1) REMPI via the $R(12)$ branch of the $f\,^1\Pi$ state of NH for the 0–0 and 0–1 vibrational bands. Terms up to β_6 (with $\beta_0 = 1$) are included in the photoelectron angular distributions, and $\theta = 0$ is vertical.

is observed and predicted theoretically, similar to that observed in photoionization of the $D\,^2\Sigma^-$ ($3p\sigma$) state of OH (Ref. 3). The photoelectron angular distributions are dependent on the rotational level of the ion indicating that they result from different partial wave components of the photoelectron matrix element. Since the Λ doublets of the $X\,^2\Pi$ ionic states are not resolved, the selection rules of Eqs. (5) and (6) show that each ΔN rotational transition and associated photoelectron angular distribution have both even and odd partial wave contributions to the photoelectron matrix element. Slightly asymmetrical spectra about the $\Delta N = 0$ transition are seen in both the observed and calculated spectra, and arise from small differences in photoelectron energies in this high-J limit. The physical origin of opposite "skewing" in the experimental spectra compared with theory is not clear. This discrepancy with theory may arise from the inadequacy of the Hartree–Fock model, as noted in the case of OH (Ref. 3). Further theoretical and experimental investigations such as zero-kinetic energy (ZEKE) or laser-induced fluorescence (LIF) studies may be required to understand this phenomenon. Essentially, Franck–Condon distributions are observed for the 0–0 and 0–1 vibrational transitions and predicted in Fig. 2. Non-Franck–Condon behavior has been predicted for ion vibrational distributions for (3 + 1) REMPI from the $X\,^3\Sigma^-$ ground state via the $3\,^3\Pi(3p\sigma)$ Rydberg state of NH, particularly for higher vibrational levels, due to orbital evolution of the $3p\sigma$ orbital in combination with Cooper minima.[9] Note, however, that in Fig. 2 the photoelectron angular distributions for the $\Delta N = \pm 1$ peaks are quite different for the $v^+ = 0$ and 1 vibrational transitions, indicating an R dependence of the transition moment, even at this low vibrational excitation.

In Table II we tabulate the ℓ contributions to the rotational branching ratios of Fig. 2(b) for the 0–0 transition. Note that each transition has been normalized so that a sum over all components yields unity (100%). Surprisingly, ΔN = even transitions have a very weak contribution from the even partial wave components of the photoelectron matrix element, whereas ΔN = odd peaks have dominant even partial wave contributions. To further clarify the underlying photoionization dynamics, we show rotational ion distributions for separate parity components of the Λ doublet of the ionic rotational levels in Fig. 3 for the $X\,^2\Pi_{1/2}(v^+ = 0)$ [Fig. 3(a)] and $X\,^2\Pi_{3/2}(v^+ = 0)$ [Fig. 3(b)] spin–orbit states of the ion. These spectra correspond to transitions from the e level of the $f\,^1\Pi$ state, and have been normalized to the most intense transition. A strongly parity-favored ion distribution is seen with about 85% population in the (−) parity component (solid bar) of the Λ doublet of the J^+ rotational levels, which is due to odd partial wave contributions to the photoelectron matrix element. These odd partial wave components mainly contribute to the e component of the J^+ rotational levels (ΔN = even) of the $X\,^2\Pi_{1/2}$ ion and to the f component of the J^+ rotational levels (ΔN = even) for the $X\,^2\Pi_{3/2}$ ion. The 15% population in the (+) parity component (cross-hatched bar) of the Λ doublet arises from even partial wave contributions. Note that even partial wave

TABLE II. Partial wave contributions to rotational branching ratios of Fig. 2(b) for the 0–0 vibrational band resulting from (2 + 1) REMPI via the $R(12)$ branch of the $f\,^1\Pi$ state of NH. Each ΔN transition has been normalized to unity (100%). The $\Delta N = 0$ transition corresponds to $N^+ = 13$.

	ΔN						
	−3	−2	−1	0	1	2	3
$\ell = 0$	0.00	0.09	45.18	0.15	49.25	0.06	0.00
$\ell = 1$	0.54	9.44	3.53	75.59	3.14	10.57	0.31
$\ell = 2$	85.38	0.57	40.46	0.26	38.22	0.39	89.49
$\ell = 3$	9.44	89.85	9.88	23.99	8.39	88.94	5.24
$\ell = 4$	4.61	0.03	0.95	0.01	0.99	0.02	4.95

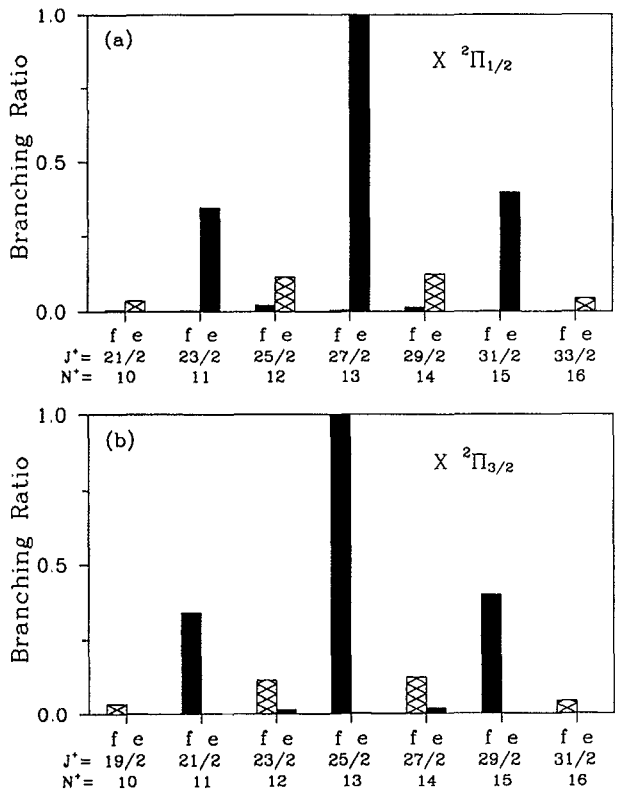

FIG. 3. Rotational ion distributions for the Λ doublets of the J^+ rotational levels of Fig. 2 for the (a) $X\,^2\Pi_{1/2}(v^+=0)$ and (b) $X\,^2\Pi_{3/2}(v^+=0)$ spin–orbit states of the ion.

contributions would be expected to be dominant for photoionization of a $3p\sigma$ orbital in an atomiclike picture, i.e., $p\rightarrow ks$, kd transitions.

Recently, Λ-doublet resolved rotational ion distributions deduced from LIF spectra for (2 + 1) REMPI via the $S(2)$ branch of the $F\,^1\Delta_2(5p\pi)$ Rydberg state of HBr have been measured by Xie and Zare.[29,30] About 18% population, which would arise from the odd partial wave contributions to the photoelectron matrix element, is seen in the (+) parity component of the Λ doublet of the J^+ rotational levels. Similar distributions were also predicted for (2 + 1′) REMPI via the $S(0)$ branch of the $F\,^1\Delta_2(4p\pi)$ state of HCl (Refs. 31 and 32). Wang and McKoy[30,32] have shown that this behavior arises from strong ℓ mixing in the electronic continuum, caused by the nonspherical molecular potential. Note that the abnormal distributions seen in Figs. 2 and 3 *cannot* be simply explained by this mechanism, since ℓ = even partial wave contributions to the photoelectron matrix element are much smaller for the $f\,^1\Pi$ state of NH. By analogy to photoionization of the D states of OH (Ref. 3) and NO (Refs. 4 and 5), the minima in the $\ell=2$ wave of the $k\sigma$ and $k\pi$ channels (see Fig. 1) play an essential role in these anomalous photoelectron spectra. This depletion of the $\ell=2$ continuum wave in the vicinity of the minima subsequently enhances the relative importance of the p and f waves. The strong $\Delta N=0$ peak is associated mainly with the p (76%) and f (24%) wave components of the photoelectron matrix element. At $R_e=2.06\,a_0$, the $3p\sigma(5\sigma)$ orbital of the $f\,^1\Pi$ state has 24.8% s and 67.2% p character, and the $3s\sigma\rightarrow kp\sigma$ transition also contributes substantially to the photoelectron matrix element. The continuum f ($\ell=3$) wave, which primarily arises from strong ℓ mixing in the electronic continuum, is also important and entirely molecular in origin. It contributes mainly to the $\Delta N=\pm 2$ ($\sim$90%) peaks. Thus, Cooper minima, orbital evolution, and strong ℓ mixing in the electronic continuum account for the dominant $\Delta N=$ even transitions observed in experimental and theoretical spectra (Fig. 2).

Closer examination of the rotational ion distributions of Fig. 3 reveals that the $\Delta N=$ odd (even) transitions have very small contributions from odd (even) partial wave components of the photoelectron matrix element. To understand this feature, we also examined the rotational ion distributions of the Λ doublet of the J^+ rotational levels resulting from (2 + 1′) REMPI via the $R(12)$ rotational branch of the $f\,^1\Pi$ state at six photoelectron kinetic energies between 0.05 eV and 4.5 eV (not shown). Even though the rotational branching ratios vary as a function of kinetic energy due to the formation of Cooper minima,[5] this feature of the Λ-doublet resolved spectra remains the same. On the other hand, the rotational ion distributions for photoionization of the $g\,^1\Delta(3p\pi)$ state (discussed below) show comparable contributions from even (odd) partial wave components for $\Delta N=$ even (odd) transitions. Consequently, the observed $\Delta N=\pm 1$ peaks are more intense than the $\Delta N=\pm 2$ for the g state, but this is not the case for the f state (cf. Figs. 2 and 6). For photoionization of the $f\,^1\Pi$ state of NH, examination of $D_\ell^{(-)}$ for various channels reveals that a strong destructive interference occurs between various ionization channels for each partial wave for the $f(e)$ components of the J^+ rotational levels of the $X\,^2\Pi_{1/2}$ ($X\,^2\Pi_{3/2}$) spin–orbit state of the ion (see Fig. 3). This interference arises from the relative phase difference of the individual partial wave components $D_\ell^{(-)}$ for the different photoelectron continua. Note that rotational branching ratios for the $X\,^2\Pi_{1/2}$ and $X\,^2\Pi_{3/2}$ ions of Fig. 3 are similar, indicating that spin–orbit interactions do not play a role here. On the other hand, these interactions are very important for photoionization of the F state of HCl (Ref. 32).

In Fig. 4 we show measured [Fig. 4(a)] and calculated [Fig. 4(b)] photoelectron spectra along with calculated photoelectron angular distributions resulting from (2 + 1) REMPI via the $S(9)$ rotational branch of the $f\,^1\Pi(N=11)$ Rydberg state of NH for the 0–0 and 0–1 vibrational bands. The ion distributions are similar to those of Fig. 2 [$R(12)$ branch] in this high-J limit. However, photoelectron angular distributions show differences which can be shown to be due to differences in the alignment of the $f\,^1\Pi$ state for the $S(9)$ and $R(12)$ branches.

B. (2+1) REMPI via the $g\,^1\Delta$ Rydberg state of NH

In Fig. 5 we show the magnitude $|D_\ell^{(-)}|$ of the photoelectron matrix element as a function of photoelectron kinetic energy for photoionization channels $3p\pi\rightarrow k\sigma(^1\Pi)$ [Fig. 5(a)], $3p\pi\rightarrow k\pi(^1\Delta)$ [Fig. 5(b)], $3p\pi\rightarrow k\delta(^1\Pi)$ [Fig. 5(c)], and $3p\pi\rightarrow k\delta(^1\Phi)$ [Fig. 5(d)] via the $g\,^1\Delta(3p\pi)$

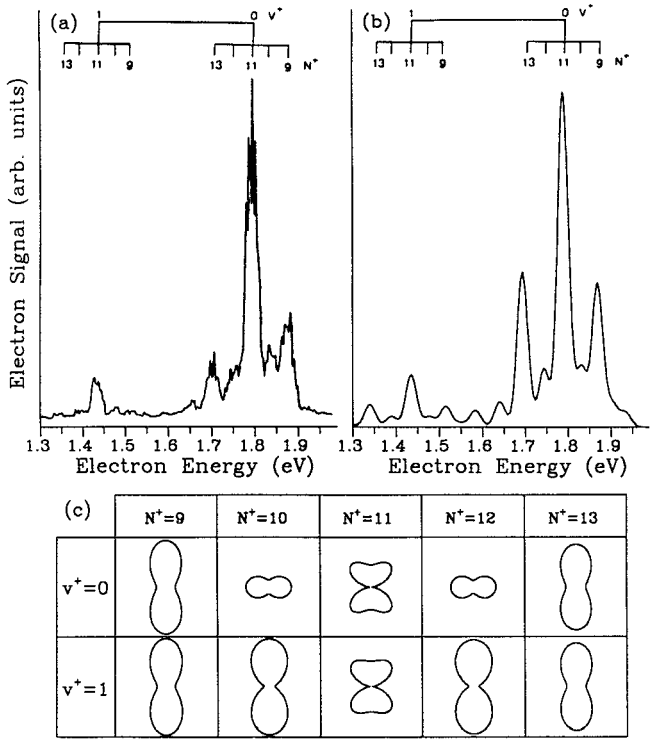

FIG. 4. The same as in Fig. 2 except for (2 + 1) REMPI via the $S(9)$ branch of the $f\,^1\Pi(v=0)$ state of NH.

Rydberg state of NH. Three Cooper minima are clearly seen in the $\ell = 2$ wave of the $k\pi(^1\Delta)$, $k\delta(^1\Pi)$, and $k\delta(^1\Phi)$ channels. The actual sign changes in D_ℓ^P are also shown in the insets of Fig. 5(b)–(d). Strong ℓ mixing in the electronic continuum is reflected in the significant p and f partial wave components of the photoelectron matrix element. The shift in the positions of the Cooper zero in D_ℓ^P and minima in $|D_\ell^{(-)}|$ due to renormalization is evident in the $k\pi(^1\Delta)$ channel.

In Fig. 6 we show the measured [Fig. 6(a)] and calculated [Fig. 6(b)] photoelectron spectra along with the calculated photoelectron angular distributions [Fig. 6(c)] resulting from (2 + 1) REMPI via the $Q(16)$ rotational branch of the $g\,^1\Delta(3p\pi)$ Rydberg state of NH for the 0–0 and 0–1 vibrational bands. The calculated spectra are convoluted with a Gaussian detection function having an FWHM of 30 meV. In these calculations, the alignment of the g state was determined by including five $^1\Delta$, six $^1\Pi$, and two $^1\Phi$ virtual states (obtained from IVO calculations) in evaluating the B_0 and B_2 factors of Eq. (4). Inclusion of eight $^1\Delta$, ten $^1\Pi$, and four $^1\Phi$ virtual states in the calculation of the alignment led to no significant changes in the rotational photoelectron spectra. Franck–Condon distributions are seen in both the experimental and theoretical spectra. The agreement between the calculated and measured spectra is good. The calculated $\Delta N = 0$ peak is somewhat more intense than

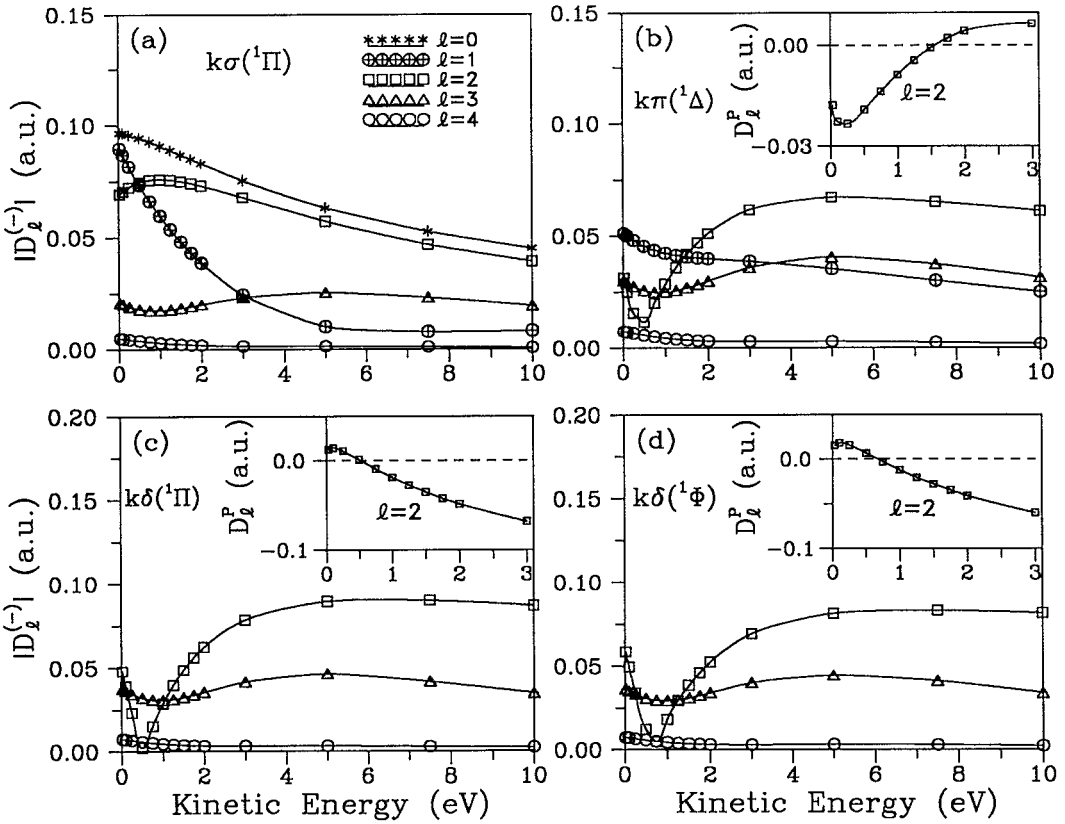

FIG. 5. Magnitude $|D_\ell^{(-)}|$ of the partial wave components of the photoelectron matrix element for photoionization of the $g\,^1\Delta(3p\pi)$ Rydberg state of NH for the (a) $3p\pi \rightarrow k\sigma(^1\Pi)$, (b) $3p\pi \rightarrow k\pi(^1\Delta)$, (c) $3p\pi \rightarrow k\delta(^1\Pi)$, and (d) $3p\pi \rightarrow k\delta(^1\Phi)$ ionization channels. The inset shows the principal-value dipole amplitude D_ℓ^P for the $\ell = 2$ component.

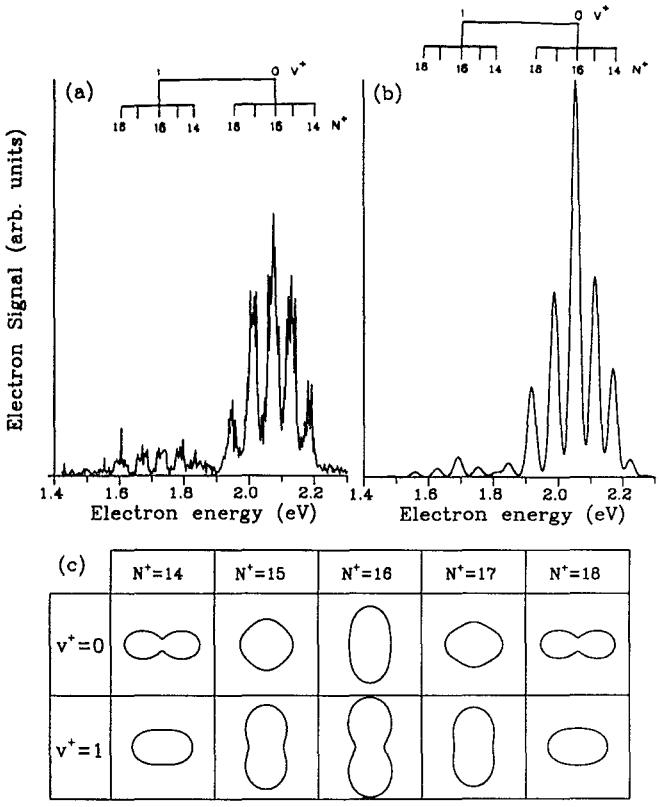

FIG. 6. The same as in Fig. 2 except for (2 + 1) REMPI via the $Q(16)$ branch of the $g\,^1\Delta(v=0)$ state of NH.

in the measured spectra. Note that the $\Delta N = \pm 2$ peaks here have almost the same intensity in both the experimental and theoretical spectra, in contrast to the strongly (and opposite) skewed spectra observed for photoionization of the $f\,^1\Pi$ state (cf. Figs. 3 and 6).

According to parity selection rules of Eqs. (5) and (6), each ΔN transition and associated photoelectron angular distribution should arise from both even and odd partial wave contributions to the photoelectron matrix element. The photoelectron angular distributions of Fig. 6(c) clearly depend on vibrational and rotational levels of the ion. These distributions reflect the important angular momentum components of the photoelectron orbitals. We tabulate the ℓ contributions to rotational branching ratios for the 0–0 vibrational band of Fig. 6 in Table III. Clearly, even partial wave contributions are dominant for most transitions (except for $\Delta N = \pm 3$), as expected for photoionization of a $3p\pi$ orbital in an atomiclike picture. To further understand the underlying photoionization dynamics, we show the ion rotational distributions of the Λ doublet of the J^+ rotational levels in Fig. 7 resulting from (2 + 1) REMPI via the $Q(16)$ branch of the e level of the $g\,^1\Delta$ state for the 0–0 vibrational band. A strongly parity-favored distribution is also seen with about 81% population in the (−) parity component (solid bar) of the Λ doublet of the J^+ rotational levels, which arises from even partial wave contributions to the photoelectron matrix element. The 19% population seen in the (+) parity components (cross-hatched bar) has contributions from the odd angular momentum components of the photoelectron matrix element. This is similar to photoionization of the $F\,^1\Delta_2$ Rydberg states of HBr (Refs. 29 and 30) and HCl (Refs. 31 and 32). Note that the photoelectron kinetic energy for (2 + 1) REMPI via the g state lies somewhat above that of the Cooper minima seen in Fig. 5, which precludes dominance of odd partial waves as in the f state. The ΔN = even (odd) transitions have comparable contributions from the even (odd) continuum waves (cf. Figs. 3 and 7). Also, spin–orbit interactions are not important for photoionization of the g state (cf. Figs. 3 and 7).

In Fig. 8 we show the measured[6] [Fig. 8(a)] and calculated [Fig. 8(b)] photoelectron spectra along with the calculated photoelectron angular distributions [Fig. 8(c)] resulting from (2 + 1) REMPI via the $Q(14)$ rotational branch of the $g\,^1\Delta(v=1)$ Rydberg state of NH. The calculated spectra and photoelectron angular distributions are similar to those of Fig. 6 in which the $v=0$ vibrational level of the g state is accessed. Franck–Condon vibrational transitions are predicted here using the Hartree–Fock model, since the angular momentum composition of the $3p\pi$ Rydberg orbital of the g state varies slightly with internuclear distance. The change of vibrational levels ($v = 0 \rightarrow 1$) does not affect the corresponding photoelectron matrix element much. The observed strong non-Franck–Condon distribution seen in measured spectra [Fig. 8(a)] may be due to an avoided crossing with another state. A strong perturbation from other states has been predicted by Goldfield and Kirby,[27] who studied the electronic structure of NH using configuration-interaction methods. The agreement between the measured and calculated rotational distributions of the $\Delta v = 0$ band is good. Additional studies beyond the present one-electron Hartree–Fock model may be required to ac-

TABLE III. Partial wave contributions to rotational branching ratios of Fig. 6(b) for the 0–0 vibrational band resulting from (2 + 1) REMPI via the $Q(16)$ branch of the $g\,^1\Delta$ state of NH. Each ΔN transition has been normalized to unity (100%). The $\Delta N = 0$ transition corresponds to $N^+ = 16$.

	ΔN						
	−3	−2	−1	0	1	2	3
$\ell = 0$	0.00	0.28	39.15	65.81	34.48	0.22	0.00
$\ell = 1$	0.00	1.02	19.70	12.88	16.46	0.56	0.00
$\ell = 2$	31.76	86.60	35.68	19.94	42.50	85.57	39.06
$\ell = 3$	67.65	12.10	5.47	0.81	6.54	13.65	60.94

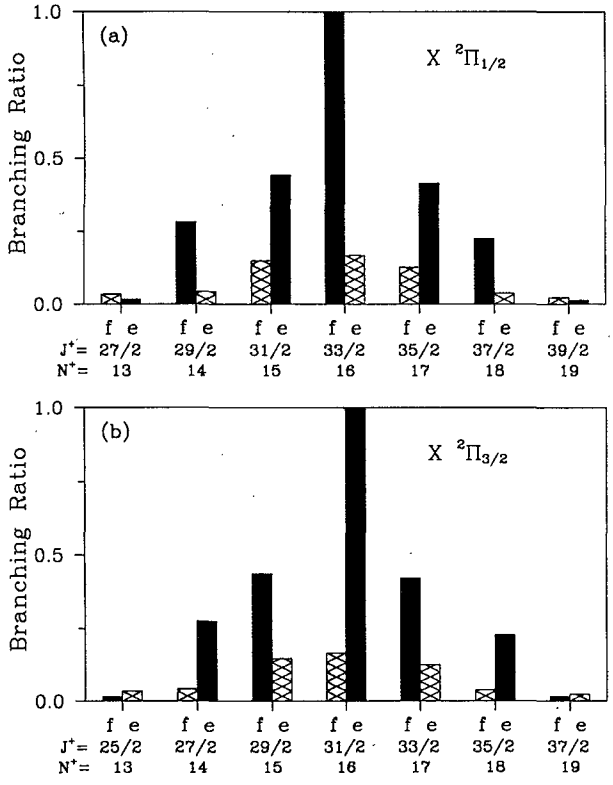

FIG. 7. The same as in Fig. 3 except for J^+ rotational levels of Fig. 6.

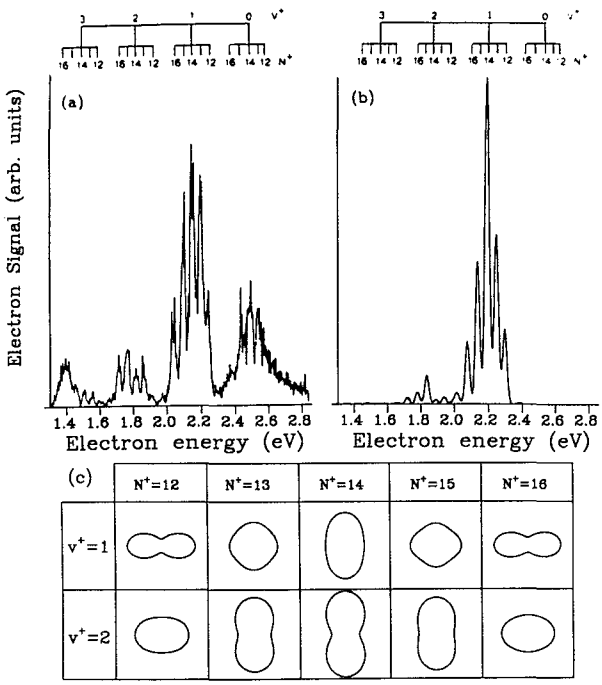

FIG. 8. The same as in Fig. 2 except for $(2+1)$ REMPI via the $Q(14)$ branch of the $g\,^1\Delta(v=1)$ state of NH.

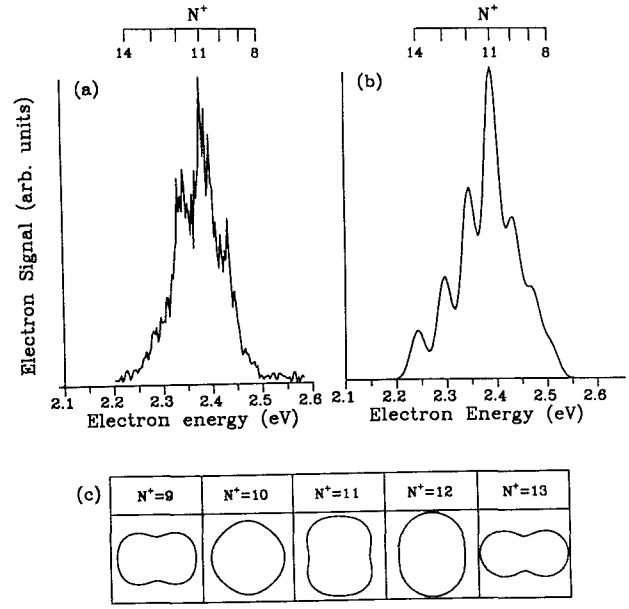

FIG. 9. The same as in Fig. 2 except for $(2+1)$ REMPI via the $R(10)$ branch of the $h\,^1\Sigma^+(3p\pi)$ state of NH.

count for this observed strong non-Franck–Condon distribution.

C. (2+1) REMPI via the $h\,^1\Sigma^+$ Rydberg state of NH

Previously, the h state was identified and assigned as $^1\Sigma$ symmetry,[26] and the present calculation further establishes its assignment as $^1\Sigma^+$. In Fig. 9 we show the observed [Fig. 9(a)] and calculated [Fig. 9(b)] photoelectron spectra along with the calculated photoelectron angular distributions [Fig. 9(c)] for $(2+1)$ REMPI via the $R(10)$ branch of the $h\,^1\Sigma^+(3p\pi)$ state of NH. The calculated spectra are convoluted with a Gaussian detection function having an FWHM of 35 meV. The amplitudes $|D_\gamma^{(-)}|$ (not shown) for the $3p\pi \rightarrow k\pi(^1\Sigma^+)$ and $3p\pi \rightarrow k\delta(^1\Pi)$ channels are very similar to those for the g state (Fig. 5), exhibiting Cooper minima at nearly the same kinetic energies. This is because the h and g states differ only in overall term symbol but have Rydberg electrons of the same spatial symmetry. Agreement between experiment and theory is satisfactory.

ACKNOWLEDGMENTS

Work at the California Institute of Technology was supported by grants from the National Science Foundation, Air Force Office of Scientific Research, and the Office of Health and Environmental Research of the U.S. Department of Energy. We acknowledge use of resources of the Jet Propulsion Laboratory/Caltech CRAY Y-MP2E/116 Supercomputer. Work at the University of Amsterdam was supported by the Netherlands Organization for Scientific Research (N.W.O.).

[1] J. W. Cooper, Phys. Rev. **128**, 681 (1962); U. Fano and J. W. Cooper, Rev. Mod. Phys. **40**, 441 (1968); A. F. Starace, in *Handbuch der Physik*, edited by M. Mehlhorn (Springer, Berlin, 1982), Vol. 31, pp. 1–121.

[2] S. T. Manson, Phys. Rev. A **31**, 3698 (1985); A. Z. Msezane and S. T. Manson, Phys. Rev. Lett. **48**, 473 (1982).
[3] E. de Beer, C. A. de Lange, J. A. Stephens, K. Wang, and V. McKoy, J. Chem. Phys. **95**, 714 (1991).
[4] K. S. Viswanathan, E. Sekreta, E. R. Davidson, and J. P. Reilly, J. Phys. Chem. **90**, 5078 (1986).
[5] K. Wang, J. A. Stephens, and V. McKoy, J. Chem. Phys. **95**, 6456 (1991).
[6] E. de Beer, M. Born, C. A. de Lange, and N. P. C. Westwood, Chem. Phys. Lett. **186**, 40 (1991).
[7] J. A. Stephens and V. McKoy, Phys. Rev. Lett. **62**, 889 (1989).
[8] J. A. Stephens and V. McKoy, J. Chem. Phys. **93**, 7863 (1990).
[9] K. Wang, J. A. Stephens, and V. McKoy, J. Chem. Phys. **93**, 7874 (1990).
[10] K. Wang and V. McKoy, J. Chem. Phys. **95**, 4977 (1991).
[11] H. Rudolph and V. McKoy, J. Chem. Phys. **91**, 7995 (1989); **93**, 7054 (1990).
[12] J. Xie and R. N. Zare, J. Chem. Phys. **93**, 3033 (1990).
[13] S. N. Dixit and V. McKoy, Chem. Phys. Lett. **128**, 49 (1986).
[14] G. Raseev and N. Cherepkov, Phys. Rev. A **42**, 3948 (1990).
[15] B. G. Koenders, D. M. Wieringa, K. Drabe, and C. A. de Lange, Chem. Phys. **118**, 113 (1987).
[16] P. Kruit and F. H. Read, J. Phys. E **16**, 313 (1983).
[17] K.-H. Gericke, T. Haas, M. Lock, R. Theinl, and F. J. Comes, J. Phys. Chem. **95**, 6104 (1991).
[18] H. H. Nelson and J. R. McDonald, J. Chem. Phys. **93**, 8777 (1990).
[19] J. B. Halpern, H. Zacharias, and R. Wallenstein, J. Mol. Spectrosc. **79**, 1 (1980).
[20] M. Dubs, U. Brühlmann, and J. R. Huber, J. Chem. Phys. **84**, 3106 (1986).
[21] J. M. Brown, J. T. Hougen, K.-P. Huber, J. W. C. Johns, I. Kopp, H. Lefebvre-Brion, A. J. Merer, D. A. Ramsay, J. Rostas, and R. N. Zare, J. Mol. Spectrosc. **55**, 500 (1975).
[22] R. R. Lucchese, G. Raseev, and V. McKoy, Phys. Rev. A **25**, 2572 (1982).
[23] R. R. Lucchese, K. Takatsuka, and V. McKoy, Phys. Rep. **131**, 147 (1986).
[24] W. J. Hunt and W. A. Goddard, Chem. Phys. Lett. **3**, 414 (1969).
[25] T. H. Dunning, Jr., J. Chem. Phys. **53**, 2823 (1970); **55**, 3958 (1971).
[26] R. D. Johnson III and J. W. Hudgens, J. Chem. Phys. **92**, 6420 (1990).
[27] E. M. Goldfield and K. P. Kirby, J. Chem. Phys. **87**, 3986 (1987).
[28] A Rydberg orbital with dominant p character could occur at $R \geqslant 3.5\ a_0$, due to the avoided crossing with another potential curve. See Ref. 27.
[29] J. Xie and R. N. Zare, Chem. Phys. Lett. **159**, 399 (1989).
[30] K. Wang and V. McKoy, J. Chem. Phys. **95**, 7872 (1991).
[31] K. S. Haber, Y. Jiang, G. Bryant, E. R. Grant, and H. Lefebvre-Brion, Phys. Rev. A **44**, 5331 (1991).
[32] K. Wang and V. McKoy, J. Chem. Phys. **95**, 8718 (1991).